SUPPLEMENTAL MATERIALS AND METHODS

Synthesis of M_3, [^{18}F]M_3 and the precursor 1

General. Proton and carbon nuclear magnetic resonance (^{1}H NMR, ^{13}C NMR) spectra were recorded on Bruker Ultra Shield-300 (300 MHz) or Varian INOVA-400 (400 MHz) instruments. Chemical shifts are given in parts per million (ppm) with tetramethylsilane as an internal standard. Abbreviations used are as follows: s = singlet, d = doublet, t = triplet, q = quartet, m = multiplet, dd = doublets of doublet, brs = broad singlet. Coupling constants (*J* values) are given in hertz (Hz). The acidic protons of diketones, carboxylic acids, alcohols, or anilines were not frequently observed in ^{1}H NMR spectra. Elemental analyses were performed by Takeda Analytical Laboratories Ltd. or Toray Research Center, Inc. or Sumika Chemical analysis Service, Ltd.. Chemical intermediates were characterized by ^{1}H NMR and/or ^{13}C NMR and/or mass spectral data. Purity data were collected by an HPLC with Corona CAD(Charged Aerosol Detector) or photo diode array detector. The column was a Capcell Pak C18AQ (50 mm x 3.0 mm I.D., Shiseido, Japan) or L-column 2 ODS (30 mm x 2.0 mm I.D., CERI, Japan) with a temperature of 50 °C and a flow rate of 0.5 mL/min. Mobile phase A and B under a neutral condition were a mixture of 50 mmol/L Ammonium acetate, water and acetonitrile (1:8:1, v/v/v) and a mixture of 50 mmol/L ammonium acetate and acetonitrile (1:9, v/v), respectively. The ratio of mobile phase B was increased linearly from 5% to 95% over 3 min, 95% over the next 1 min. Mobile phase A and B under an acidic condition were a mixture of 0.2% formic acid in

10 mmol/L ammonium formate and 0.2% formic acid in acetonitrile, respectively. The ratio of mobile phase B was increased linearly from 14% to 86% over 3 min, 86% over the next 1 min. The HPLC analyses were performed using a Shimadzu UFLC instrument, equipped with a L-column 2 ODS (3.0 × 50 mm, 2 μm) column, eluting with a gradient of 5–90% solvent B in solvent A (solvent A was 0.1% TFA in water, and solvent B was 0.1% TFA in acetonitrile), at a flow rate of 1.2 mL/min, with UV detection at 220 nm. Reagents and solvents were obtained from commercial sources and used without further purification. Reaction progress was determined by thin layer chromatography (TLC) analysis on Merck Kieselgel 60 F254 plates or Fuji Silysia NH plates. Chromatographic purification was performed on silica gel columns [(Merck Kieselgel 60, 70–230 mesh size or 230–400 mesh size, Merck) or (Chromatorex NH-DM 1020, 100–200 mesh size)] or on Purif-Pack (SI or NH, particle size: 60 μm, Fuji Silysia Chemical, Ltd.). M_3 and the precursor 1 were synthesized as shown in Supplemental Scheme 1. Radiosynthesis of [^{18}F]M_3 was conducted as shown in supplemental Scheme 2.

(*rac*)-*tert*-Butyl 4-(1-(3-iodophenyl)-5-oxopyrrolidin-3-yl)piperazine-1-carboxylate (4). To a mixture of **2** (1.41 g, 4.68 mmol), **3** (1.05 g, 5.62 mmol), acetic acid (0.804 ml, 14.1 mmol) in THF (dry) (20 mL) was added $NaBH_3CN$ (0.883 g, 14.1 mmol) at room temperature. The mixture was stirred at 50 °C under N_2 overnight. The mixture was poured into K_2CO_3 aqueous solution and extracted with EtOAc. The organic layer was separated, washed with brine, dried

over Na_2SO_4 and concentrated in vacuo. The residue was purified by column chromatography (NH silica gel, eluted with 20%- 60% EtOAc in hexane) to give **4** (0.950 g, 2.02 mmol, 43 %) as a white powder. ^{1}H NMR (300 MHz, DMSO-*d*$_6$) δ 1.39 (9H, s), 2.26-2.46 (5H, m), 2.62-2.75 (1H, m), 3.12-3.25 (1H, m), 3.32 (4H, s), 3.61-3.75 (1H, m), 3.86-3.98 (1H, m), 7.11-7.22 (1H, m), 7.44-7.53 (1H, m), 7.61-7.70 (1H, m), 8.07-8.13 (1H, m). MS (ESI/APCI) *m*/*z* 472.0 $[M+H]^+$.

(*R*)-*tert*-Butyl 4-(1-(3-iodophenyl)-5-oxopyrrolidin-3-yl)piperazine-1-carboxylate (5). 4 (950 mg, 2.02 mmol) was fractionated by HPLC (column: CHIRALCEL ASH, 50 mmID x 500 mmL, 5 μm, mobile phase: Hexane/Ethanol = 750/250, pressure: 0.2 Mpa, flow rate: 80 mL/min, temperature: 30 °C, detection: UV 220 nm) and the obtained fraction was concentrated under reduced pressure to give **5** (420 mg, 0.891 mmol, 44% yield, > 99% ee) having a short retention time. MS (ESI/APCI) *m*/*z* 472.0 $[M+H]^+$.

(*R*)-*tert*-Butyl 4-(1-(3-(2-fluoro-4-methylpyridin-3-yl)phenyl)-5-oxopyrrolidin-3-yl)piperazine-1-carboxylate (6). The mixture of **5** (160 mg, 0.34 mmol), $Pd_2(dba)_3$ (15.5 mg, 0.017 mmol), 1 M aqueous CsF solution (1.02 mL, 1.02 mmol), (2-fluoro-4-methylpyridin-3-yl)boronic acid (105 mg, 0.68 mmol), *N*-phenyl-2-(di-*tert*-butylphosphino)indol (22.9 mg, 0.068 mmol) and DME (3.0 mL) was stirred at 80 °C under N_2 for 2 h. The mixture was

poured into water at room temperature and extracted with EtOAc. The organic layer was separated, washed with brine, dried over $MgSO_4$ and concentrated in vacuo. The residue was purified by column chromatography (NH silica gel, eluted with 40% - 100% EtOAc in hexane) to give **6** (151 mg, 0.332 mmol, 98 %). ^{1}H NMR (300 MHz, DMSO-d_6) δ 1.39 (9H, s), 2.20 (3H, s), 2.31-2.49 (5H, m), 2.52-2.58 (1H, m), 2.61-2.74 (1H, m), 3.13-3.24 (1H, m), 3.28-3.36 (3H, m),3.69-3.82 (1H, m), 3.89-3.99 (1H, m), 7.06-7.16 (1H, m), 7.31-7.38 (1H, m), 7.43-7.54 (1H, m), 7.62-7.65 (1H, m), 7.74-7.82 (1H, m), 8.07-8.16 (1H, m). MS (ESI/APCI) *m*/*z* 355.1 $[M\text{-}Boc+H]^+$.

(*R*)-1-(3-(2-fluoro-4-methylpyridin-3-yl)phenyl)-4-(piperazin-1-yl)pyrrolidin-2-one dihydrochloride (M3). The mixture of **6** (151 mg, 0.33 mmol) and 4 M HCl/EtOAc solution (2.0 ml, 8.0 mmol) was stirred at room temperature under a dry atmosphere for 5 h. The mixture was concentrated in vacuo. The solid was crystallized from EtOH-EtOAc-heptane to give **M3** (102 mg, 0.239 mmol, 72 %). ^{1}H NMR (300 MHz, DMSO-d_6) δ 2.21 (3H, s), 2.77-3.04 (3H, m), 3.05-3.45 (8H, m), 3.75-3.98 (1H, m), 3.98-4.11 (1H, m), 4.14-4.22 (1H, m), 7.16 (1H, d, J = 7.2 Hz), 7.36 (1H, d, J = 4.9 Hz), 7.53 (1H, t, J = 8.1 Hz), 7.61 (1H, s), 7.76-7.87 (1H, m), 8.13 (1H, d, J = 4.9 Hz), 9.35 (2H, brs). MS (ESI/APCI) *m*/*z* 355.3 $[M+H]^+$. HPLC purity: 98.3%.

(*R*)-*tert*-Butyl 4-(5-oxo-1-(3-(4,4,5,5-tetramethyl-1,3,2-dioxaborolan-2-yl)phenyl)pyrrolidin-3-yl)piperazine-1-carboxylate (7). To a solution of 4,4,4',4',5,5,5',5'-octamethyl-2,2'-bi(1,3,2-dioxaborolane) (145 mg, 0.57 mmol), **5** (224 mg, 0.48 mmol) and AcOK (140 mg, 1.43 mmol) in DMF (4 mL) was added $PdCl_2$(dppf) (34.8 mg, 0.048 mmol) at ambient temperature. The mixture was stirred at 100 °C under N_2 for 1 h. The mixture was poured into water and extracted with EtOAc. The organic layer was separated, washed with brine, dried over Na_2SO_4 and concentrated in vacuo. The residue was purified by column chromatography (silica gel, eluted with 0% - 10% MeOH in EtOAc) to give **7** (150 mg, 0.318 mmol, 67.0 %). ^{1}H NMR (300 MHz, DMSO-d_6) δ 1.30 (12H, s), 1.39 (9H, s), 2.30-2.48 (5H, m), 2.58-2.71 (1H, m), 3.11-3.27 (1H, m), 3.28-3.36 (4H, m), 3.66-3.78 (1H, m), 3.87-3.99 (1H, m), 7.33-7.47 (2H, m), 7.68-7.77 (1H, m), 7.90-7.94 (1H, m). MS (ESI/APCI) *m*/*z* 472.3 $[M+H]^+$.

(*R*)-*tert*-Butyl 4-(1-(3-(4-methyl-2-nitropyridin-3-yl)phenyl)-5-oxopyrrolidin-3-yl)piperazine-1-carboxylate (1). The mixture of 3-bromo-4-methyl-2-nitropyridine (104 mg, 0.48 mmol), **7** (150 mg, 0.32 mmol), bis(di-*tert*-butyl(4-dimethylaminophenyl)phosphine)dichloropalladium (II) (21.4 mg, 0.032 mmol), 1 M aqueous Cs_2CO_3 solution (0.955 mL, 0.95 mmol) and DME (2.0 ml) was heated at 100 °C for 1 h under microwave irradiation. The residue was purified by column chromatography (NH silica

gel, eluted with 30% - 100% EtOAc in hexane. The solid was crystallized from EtOAc-IPE-heptane to give **1** (56.0 mg, 0.116 mmol, 37 %) as a white solid. ^{1}H NMR (300 MHz, DMSO-*d*$_6$) δ 1.39 (9H, s), 2.23 (3H, s), 2.38 (5H, brs), 2.52-2.57 (1H, m), 2.61-2.76 (1H, m), 3.11-3.26 (1H, m), 3.28-3.36 (3H, m), 3.67-3.82 (1H, m), 3.86-4.02 (1H, m), 7.05 (1H, d, J = 8.0 Hz), 7.48 (1H, t, J = 8.0 Hz), 7.66 (1H, brs), 7.71-7.84 (2H, m), 8.47 (1H, d, J = 4.9 Hz). MS (ESI/APCI) *m*/*z* 426.2 $[M-t\text{Bu}+H]^{+}$.

(*R*)-1-(3-(2-[^{18}F]fluoro-4-methylpyridin-3-yl)phenyl)-4-(piperazin-1-yl)pyrrolidin-2-one dihydrochloride ([^{18}F]M$_3$).

[^{18}F]fluoride was produced using a cyclotron by the ^{18}O (p, n) ^{18}F reaction on 98 atom% $H_2{}^{18}O$ (Rotem Industries, Arava, Israel) and was separated from $H_2{}^{18}O$ using the Sep-Pak Light Accell Plus QMA cartridge (Waters). The produced [^{18}F]fluoride was eluted from the cartridge with a mixture of aqueous K_2CO_3 (0.4 mg/0.2 mL) and a solution of 4,7,13,16,21,24-hexaoxa-1,10-diazabicyclo[8,8,8]-hexacosane (7.5 mg) in acetonitrile (0.2 mL) and transferred into a reaction vessel in a hot cell. The [^{18}F]fluoride solution was dried at 120 °C for 550 seconds to remove H_2O and acetonitrile. A solution of **1** (1.0 mg, 2.1 μmol, Supplemental Scheme 1) in dimethyl sulfoxide (400 μL) was combined with [^{18}F]Fluoride and heated at 150 °C for 10 min. To the mixture was added 6 M HCl aqueous solution (0.5 mL) and the mixture was stirred at room temperature for 10 min. 4 M NaOAc aqueous

solution (1.0 mL) was added into the reaction mixture, which was separated by HPLC using a YMC-Triant C18 (250 mm i.d. × 10 mm, YMC) with MeOH/H_2O (45/55, including 0.1% Et_3N) at 4.0 mL/min. The radioactive fraction corresponding to [^{18}F]M_3 (retention time = 13.5 min) was collected in a sterile flask containing polysorbate 80 (100 μL) and 25% ascorbic acid (100 μL), evaporated to dryness under vacuum, re-dissolved in 3 mL of sterile saline to obtain the final product. The identity of [^{18}F]M_3 (retention time = 17.4 min) was confirmed by analytical HPLC with M_3 using an YMC-Triant C18 (250 mm i.d. × 4.6 mm, YMC) with MeOH/H_2O (45/55, including 0.1% Et_3N) at 1.0 mL/min. The synthesis time was 67 min from the end of bombardment; radiochemical yield (decay-corrected) was 16.1% based on [^{18}F]fluoride; radiochemical purity was 97.4%, and; molar activity at the end of synthesis was 307 GBq/μmol.

Metabolites analysis of T-401 in mice

Instrument

LC/MS system consisted of ACQUITY UPLC system and SYNAPT Q-TOF mass spectrometer (Waters Corporation, Milford, MA) equipped with an electrospray ionization source.

LC/MS analysis

Aliquots of the plasma and brain pretreatment samples were separated on an ACQUITY UPLC

BEH C_{18} column (1.7 μm, 2.1 x 100 mm, Waters) using solvent A (acetonitrile/5 mM aqueous ammonium acetate (5/95, v/v)) and solvent B (acetonitrile/5 mM aqueous ammonium acetate (95/5, v/v)). At a flow rate of 0.5 mL/min, the initial elution gradient was 98% solvent A and 2% solvent B with a linear gradient to 50% solvent B over 15 min, increased to 95% solvent B, maintained for 2 min and returned to initial condition. The column was allowed to equilibrate at 2% solvent B for 3 min before the next injection. The column temperature was 40°C and the eluates were monitored with a PDA detector. The mass spectrometry was run in positive ion mode. The source setting was 1.30 kV capillary voltage, 35 V sample corn voltage, 120°C source temperature, 350°C desolvation temperature. The CE was set as ramp mode from 10 V to 40 V.

Structural identification of T-401 metabolites in mice.

Plasma and brain samples collected from mice after T-401 administration were profiled by liquid chromatography – UV detection (LC/UV) and LC/MS. Four fluoro-containing metabolites (M_1 – M_4) were observed in plasma by LC/UV, and two metabolites (M_1, M_3) were detected in the brain by LC/MS (Supplemental Figure 5). T-401 provided a protonated molecule $[M+H]^+$ at *m/z* 466 in full scan mass spectrum, and the fragment ion at *m/z* 269 and *m/z* 198 suggested pyridylphenyl pyrrolidone and thiazolyl piperazine moieties, respectively. M_1 was identified in a full scan mass spectrum at *m/z* 482, and its product ions at *m/z* 285,

267, and 198 revealed that an aliphatic hydroxyl group was substituted at the pyridylphenyl pyrrolidone moiety. M_3 was detected as a protonated molecule at *m/z* 355, suggesting a loss of the thiazolyl group. The MS/MS ion at *m/z* 87 also indicated an unsubstituted piperazine ring of M_3. A full scan mass spectrum identified M_2 at *m/z* 369, implying the introduction of a carbonyl group in M_3. A fragment ion derived from M_2 at m/z 269 indicated that its piperazine ring was oxidized. M_4 was shown as a protonated molecule at *m/z* 371, which was suggestive of hydroxylation of M_3. Product ion spectra derived from M_4 at *m/z* 285, 267, and 87 indicated that an aliphatic hydroxyl group was substituted at a biphenyl pyrrolidone moiety. The retention times of M_1, M_3 and T-401 were 3.8 min, 2.5 min, and 7.9 min, respectively, on the following HPLC condition: Atlantis T3 3 um 4.6 × 150 mm, acetonitrile: H_2O (40: 60), 1.0 mL/min, 254 nm.

Small-Animal PET studies of [^{18}F]M_3 in WT and MAGL-KO mice

PET scans of wild-type and MAGL-KO mice were performed using a micro-PET Focus 220 animal scanner (Siemens Medical Solutions USA, Knoxville, TN) designed for rodents and small monkeys, which provides 95 transaxial slices 0.815 mm (center-to-center) apart, a 19.0 cm transaxial field of view (FOV), and a 7.6 cm axial FOV (Tai et al., 2005). Before the scans, mice were anesthetized with 1.5% (v/v) isoflurane, and a 30-gauge needle connected to a 0.5 ml polypropylene syringe via a length of polyethylene tubing was inserted into the tail vein. A

dynamic emission scan in 3D acquisition mode immediately after intravenous injection of [^{18}F]M_3 (n = 4 in each group, 33.0 ± 2.4 MBq, 281-282 GBq/μmol) for 120 min. The mice were anesthetized with 1.5% (v/v) isoflurane during the emission scans. All list-mode data were sorted into 3D sinograms, which were then Fourier rebinned into 2D sinograms (frames × time: 6 × 10 sec, 30 × 8 sec, 5 × 1 min, 10 × 2 min and 12 or 18 × 5 min). Dynamic images were reconstructed with filtered back-projection using a 0.5 mm Hanning filter. ROIs were placed on multiple brain areas using PMOD software (PMOD Technologies, Zurich, Switzerland) with reference to the MRI template, and then TACs for [^{18}F]M_3 in these regions were generated. The obtained TACs were represented as standardized uptake value (SUV).

Representative baseline PET images and TACs in WT and MAGL-KO mouse brains following intravenous injection of [^{18}F]M_3 are shown in Supplemental Figure 7. [^{18}F]M_3 exhibited very poor BBB penetration and low brain uptake in the brains of these mice throughout the scanning time

***In vitro* autoradiography (ARG) study using [^{18}F]T-401 in monkey brain sections**

Frozen brain samples from rhesus monkey were cut into 20 um-thick slices by cryotome (HM560; Carl Zeiss, Germany), and the slices were mounted on slide glass (Matsunami Glass, Osaka, Japan) and stored at -80 °C until assays. These sections were reacted with 0.5 nM of [^{18}F]T-401 in 50 mM Tris-HCl buffer (pH7.4) at room temperature for 1 hour. The incubated

sections were washed with ice-cold Tris-HCl buffer for 5 min twice, warmly blow-dried and contacted to an imaging plate (BAS-MS; Fuji Film, Japan). The imaging plate data were scanned with a BAS5000 system (Fuji Film). The obtained autoradiograms were analyzed by Multi Guage (Fuji Film). The binding parameters of [^{18}F]T-401 were calculated by Prizm ver. 7 (Graph Pad) from the saturation curves. JW642 (10 μM) was simultaneously incubated with [^{18}F]T-401 to determine the nonspecific binding.

Supplemental Figure 8 shows representative *in vitro* autoradiogram of [^{18}F]T-401 on the monkey brain sections. [^{18}F]T-401 displayed heterogeneous distribution pattern of radioactivity. The highest level was observed in pallidus and occipital cortex, and moderate radioactivity was seen in cerebellum, hippocampus and thalamus (Supplemental Figure 8A). Radioactivity in these sections was completely decreased by co-incubation with 10 μM of JW642 (Supplemental Figure 8B)

In vivo Scatchard plot analysis using [^{18}F]T-401 PET data in monkey brains

The radioligand affinity for the target molecules and abundance of the binding components in the brain of a living monkey were estimated by generating a Scatchard plot using data obtained from three baseline PET scans. Briefly, the bound-to-free (B/F) ligand concentration ratio was plotted against the bound ligand concentration in four brain regions. The concentration of bound ligands was calculated as the product of V_s (= V_T - V_{ND}) and mean

plasma radioligand concentration from 60 to 90 min, which was then divided by the radioligand molar activity. The B/F ratio was determined using BP_{ND} (= V_T / V_{ND} – 1), with f_{ND} (free fraction in the brain) being assumed to be 1.

Supplemental Schemes

Supplemental Scheme 1. Synthesis of M_3 and the precursor 1.

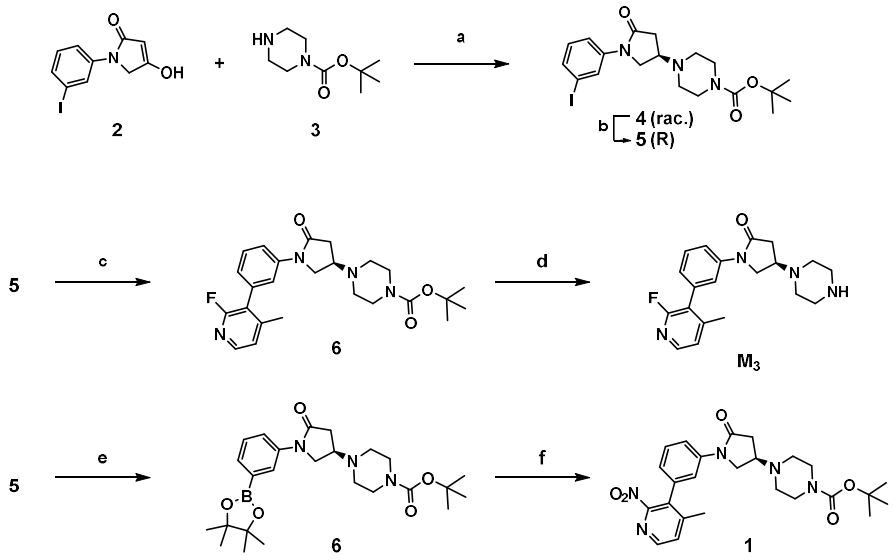

[a]Reagents and conditions: (a) $NaBH_3CN$, AcOH, THF; (b) chiral HPLC separation (Column: CHIRALPAK AS-H, *R* isomer is tR1; (c) $Pd_2(dba)_3$, CsF, (2-fluoro-4-methylpyridin-3-yl)boronic acid, *N*-phenyl-2-(di-t-butylphosphino)indol, DME; (d) HCl, EtOAc; (e) $PdCl_2(dppf)$, 4,4,4',4',5,5,5',5'-octamethyl-2,2'-bi(1,3,2-dioxaborolane), AcOK, DMF; (f) 3-bromo-4-methyl-2-nitropyridine, Bis(di-*tert*-butyl(4-dimethylaminophenyl)phosphine)dichloropalladium (II), Cs_2CO_3, DME/water.

Supplemental Scheme 2. Radiosynthesis of [^{18}F]M_3[a].

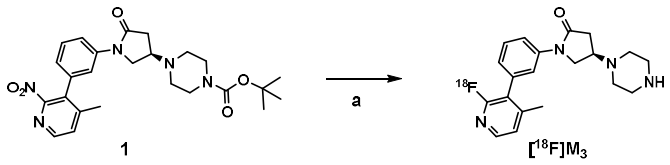

[a]Reagents and conditions: (a) K[^{18}F]F, 2,2,2-Cryptand, K_2CO_3, DMSO, 150 °C, 10 min, and then 6 M HCl solution (0.5 mL), room temperature, 10 min.; radiochemical purity, 97.4%; molar activity, 307 GBq/μmol.

Supplemental Tables

Supplemental Table 1. AIC, MSC and F values in the comparison of fitting performances between 2TCM and 2T+mCM under a blocking condition with 0.3 mg/kg of JW642 (i. v.).

	AIC		MSC		F-test
ROI	2TCM	2T+mCM	2TCM	2T+mCM	F value
FCX	59.2	58.3	4.39	4.41	2.74
STR	66.9	69.0	4.37	4.33	-0.14
CB	92.9	61.5	3.57	4.22	43.3*
OCC	52.3	51.0	4.40	4.43	3.07
HIP	99.1	81.1	3.35	3.72	22.1*
THA	67.5	65.6	4.05	4.09	3.62
Pons	88.8	87.2	3.34	3.37	3.39

*$p<0.05$ (F value > 4.06)

Supplemental Table 2. Individual kinetic parameters and their indentifiability (SE%) as calculated with the 2T+mCT model.

Baseline (M197)

	K_1		k_2		k_3		k_4		k_{trans}		V_T	
VOI	mL/min/cm^3	SE %	min^{-1}	SE %	min^{-1}	SE %	min^{-1}	SE %	min^{-1}	SE %	mL/cm^3	SE %
FCX	0.265	0.77	0.0382	7.4	0.0357	28.5	0.0535	14.5	0		11.6	0.94
STR	0.260	1.59	0.0536	15.9	0.0494	64.2	0.0724	44.3	0.0003	437	8.15	6.6
CB	0.239	0.85	0.0769	4.8	0.0353	13.0	0.0293	27.7	0.0024	101	6.85	13.4
OCC	0.248	0.91	0.0433	8.7	0.0314	41.5	0.0523	39.4	0.0009	145	9.17	7.5
HIP	0.191	1.59	0.0658	14.7	0.0642	48.8	0.0748	32.2	0.0032	45	5.41	5.7
THA	0.137	2.74	0.0481	11.9	0.0071	86.3	0.0122	130	0		4.50	25.7
Pons	0.120	3.08	0.0773	11.3	0.0181	37.2	0.0109	55.8	0		4.13	20.2

Baseline (M185)

	K_1		k_2		k_3		k_4		k_{trans}		V_T	
VOI	mL/min/cm^3	SE %	min^{-1}	SE %	min^{-1}	SE %	min^{-1}	SE %	min^{-1}	SE %	mL/cm^3	SE %
FCX	0.163	1.5	0.0233	9.37	0.0022	182	0.0050	644	0		10.1	150
STR	0.167	2.0	0.0258	6.55	0		0		0.0003	254	6.48	5.33
CB	0.180	1.6	0.0565	9.74	0.0195	37.1	0.0269	107	0.0020	283	5.50	41.8
OCC	0.185	1.3	0.0308	6.98	0.0042	78.1	0.0091	155	0		8.82	30.3
HIP	0.138	3.3	0.0508	27.2	0.0349	104	0.0434	120	0.0020	300	4.90	33.5
THA	0.148	2.5	0.0374	16.8	0.0071	363	0.0137	1110	0.0005	7722	6.02	509
Pons	0.110	2.8	0.0653	9.71	0.0089	45.9	0.0031	232	0		6.58	146

Baseline (M187)

	K_1	k_2	k_3	k_4	k_{trans}	V_T

VOI	mL/min/cm^3	SE %	min^{-1}	SE %	min^{-1}	SE %	min^{-1}	SE %	min^{-1}	SE %	mL/cm^3	SE %
FCX	0.328	1.16	0.0406	11.1	0.0304	49.0	0.0455	53.7	0		13.5	12.6
STR	0.387	3.52	0.1000	36.8	0.2028	60.6	0.0909	25.8	0		12.5	6.78
CB	0.361	0.79	0.0794	4.07	0.0344	13.1	0.0339	23.7	0.0029	60	9.17	9.73
OCC	0.329	0.77	0.0429	5.10	0.0207	27.5	0.0376	48.1	0.0007	257	11.9	12.8
HIP	0.352	3.64	0.1936	20.8	0.1906	29.6	0.0605	19.5	0.0074	62	7.55	9.14
THA	0.332	0.87	0.0635	6.21	0.0383	27.6	0.0595	25.2	0.0026	36	8.58	4.78
Pons	0.237	2.22	0.0941	13.0	0.0260	86.3	0.0676	75.8	0.0073	26	3.48	9.39

Blocking with 0.01 mg/kg JW642 (M187)

	K_1		k_2		k_3		k_4		k_{trans}		V_T	
VOI	mL/min/cm^3	SE %	min^{-1}	SE %	min^{-1}	SE %	min^{-1}	SE %	min^{-1}	SE %	mL/cm^3	SE %
FCX	0.282	0.46	0.044	6.0	0.075	19.1	0.0994	7.3	0		11.2	0.28
STR	0.391	4.99	0.308	50.6	0.967	41.6	0.1313	14.4	0		10.6	0.87
CB	0.340	0.99	0.105	6.6	0.085	17.5	0.0776	11.2	0.0061	12.9	6.77	2.43
OCC	0.269	0.51	0.038	7.0	0.027	61.7	0.1086	36.3	0.0013	22.2	8.80	1.44
HIP	0.235	2.06	0.081	18.0	0.102	43.4	0.0819	23.8	0.0013	103	6.49	4.83
THA	0.268	0.96	0.040	4.7	0.003	90.8	0.0216	92.8	0		7.62	4.16
Pons	0.202	0.85	0.089	5.5	0.026	45.8	0.0963	31.8	0.0043	10.2	2.89	2.06

Blocking with 0.03 mg/kg JW642 (M187)

	K_1		k_2		k_3		k_4		k_{trans}		V_T	
VOI	mL/min/cm^3	SE %	min^{-1}	SE %	min^{-1}	SE %	min^{-1}	SE %	min^{-1}	SE %	mL/cm^3	SE %
FCX	0.173	0.423	0.024	0.8	0		0		0		7.16	0.61
STR	0.210	1.03	0.031	2.0	0		0		0		6.76	1.50
CB	0.199	0.571	0.071	3.8	0.039	14.6	0.0508	14.3	0.0030	22.4	4.95	3.40
OCC	0.166	0.812	0.031	2.5	0		0		0.0008	38.3	5.41	1.96
HIP	0.149	2.59	0.098	29.0	0.190	59.0	0.134	22.5	0.0040	42.8	3.71	3.45
THA	0.165	0.809	0.040	2.2	0		0		0.0008	34.0	4.10	1.72
Pons	0.141	1.01	0.075	2.4	0		0		0.0049	7.30	1.89	1.82

Blocking with 0.1 mg/kg JW642 (M187)

	K_1		k_2		k_3		k_4		k_{trans}		V_T	
VOI	mL/min/cm^3	SE %	min^{-1}	SE %	min^{-1}	SE %	min^{-1}	SE %	min^{-1}	SE %	mL/cm^3	SE %
FCX	0.372	1.22	0.052	2.3	0		0		0		7.20	1.69
STR	0.418	1.60	0.065	3.1	0		0		0		6.41	2.21
CB	0.512	3.53	0.943	14.5	1.18	9.78	0.145	5.11	0.0193	14.3	4.97	1.30
OCC	0.359	0.90	0.064	1.7	0		0		0		4.97	1.30
HIP	2.077	12.8	23.24	18.0	3.27	9.76	0.070	3.80	0.0496	34.5	4.27	2.88
THA	0.338	1.32	0.074	3.0	0		0		0.0008	46.5	4.97	2.18
Pons	0.751	39.0	9.469	76.0	4.00	22.5	0.143	15.9	0.151	37.5	2.31	1.98

Blocking with 0.3 mg/kg JW642 (M187)

	K_1		k_2		k_3		k_4		k_{trans}		V_T	
VOI	mL/min/cm^3	SE %	min^{-1}	SE %	min^{-1}	SE %	min^{-1}	SE %	min^{-1}	SE %	mL/cm^3	SE %
FCX	0.196	1.72	0.126	3.51	0		0		0.0045	13.7	1.56	2.43
STR	0.211	1.82	0.151	3.55	0		0		0.0041	16.4	1.40	2.42
CB	0.288	10.4	0.887	44.1	0.804	44.8	0.261	12.3	0.0306	36.2	1.32	3.66
OCC	0.189	1.72	0.138	3.52	0		0		0.0078	8.8	1.37	2.43
HIP	0.266	28.6	1.815	100	1.68	61.8	0.240	24.5	0.0635	73.3	1.17	4.94
THA	0.215	18.0	0.511	174	1.26	217	0.591	35.4	0.0270	157	1.32	4.03
Pons	0.183	35.8	1.61	146	1.79	95.8	0.294	36.2	0.0976	110	0.808	7.11

Supplemental Table 3. K_D and B_{max} values estimated from Scatchard plot using [^{18}F]T-401-PET baseline data

ROI	K_D[nM]	B_{max}[nmol/g]
FCX	4.18	119.7
CB	1.25	41.9
OCC	3.29	88.3
HIP	1.09	32.9

Supplemental Table 4. k_{trans} values [min^{-1}] estimated with 2T+mCM under blocking with Compound 4f at a dose inducing a full MAGL occupancy.

Region	M187	M197
FCX	0.0145	0.0209
STR	0.0110	0.0161
CB	0.0202	0.0229
OCC	0.0170	0.0194
HIP	0.0186	0.0214
THA	0.0082	0.0163
Pons	0.0212	0.0267

Supplemental Figures

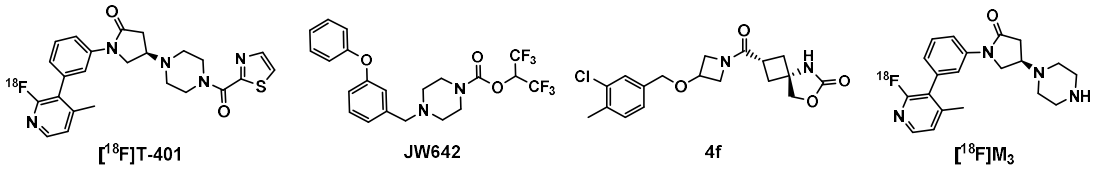

Supplemental Figure 1. Structures of [^{18}F]T-401, JW642, compound 4f and radiometabolite [^{18}F]M_3 in the mouse brain.

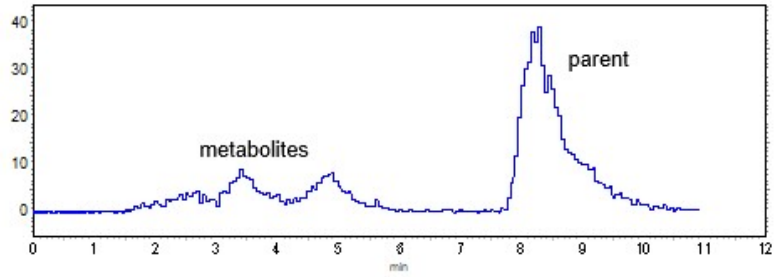

Supplemental Figure 2. A typical radiochromatogram of a monkey plasma sample at 10 min after [^{18}F]T-401 injection.

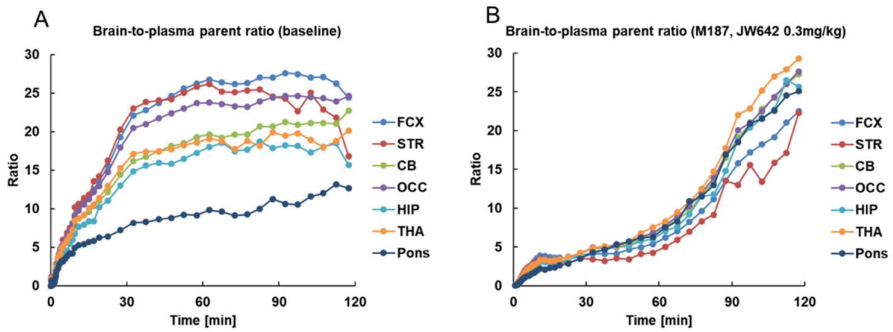

Supplemental Figure 3. Ratio of brain tissue radioactivity to plasma radioactivity of unmetabolized [^{18}F]T-401 during the PET scans at baseline (A) and following pretreatment with 0.3 mg/kg of JW642 (B). The ratio was almost plateaued in all regions except the pons at approximately 60 min after [^{18}F]T-401 injection at baseline (A), but continuously increased over time in the blockade experiment (B). FCX, frontal cortex; STR, striatum; CB, cerebellum; OCC, occipital cortex; HIP, hippocampus; THA, thalamus.

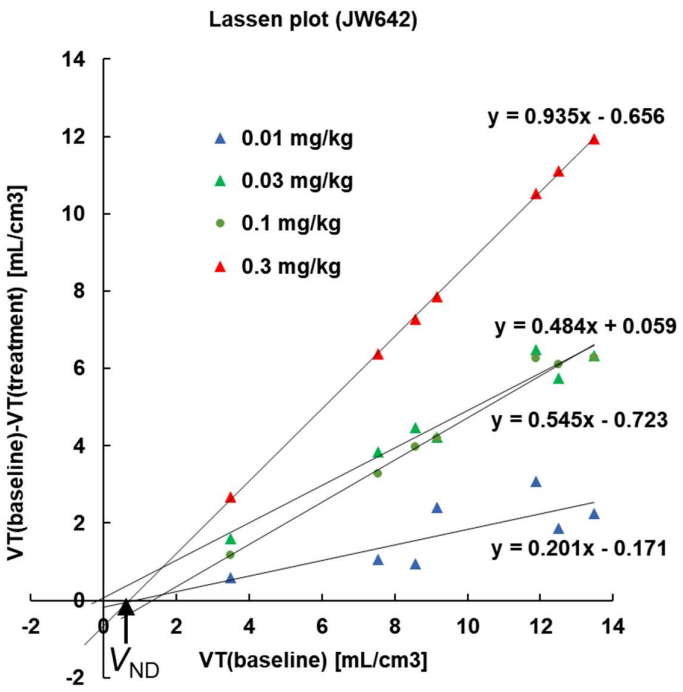

Supplemental Figure 4. A graphical analysis to determine MAGL occupancies by JW642 using V_T values estimated from [^{18}F]T-401-PET data. V_{ND} was determined by averaging x-intercepts as 0.69 mL/cm^3.

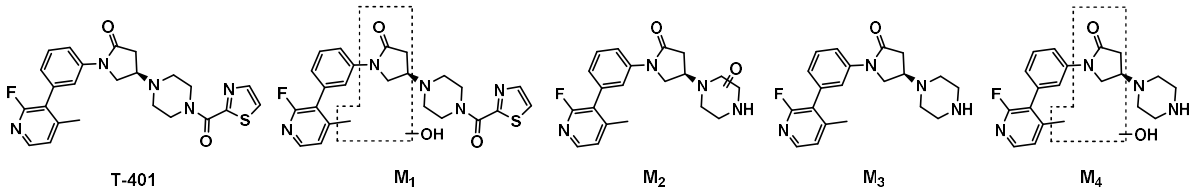

Supplemental Figure 5. Structures of T-401 and its fluoro-containing metabolites M_1-M_4. The area surrounded by the dotted line is the area expected to be hydroxylated.

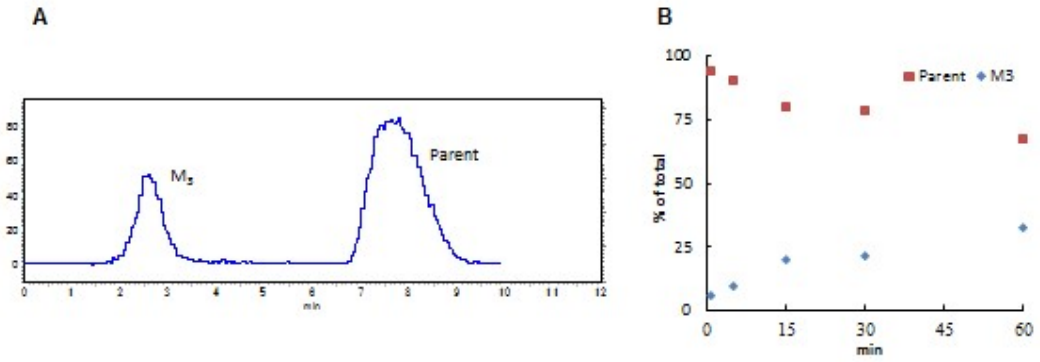

Supplemental Figure 6. (A) A typical radiochromatogram of a mouse brain sample at 15 min after [^{18}F]T-401 injection. (B) Time course changes in the fractions of [^{18}F]T-401 and [^{18}F]M_3 (n = 2).

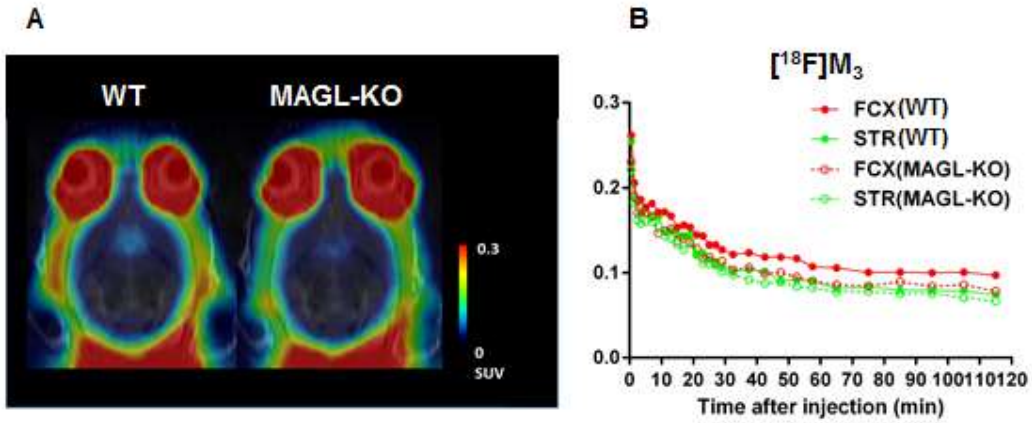

Supplemental Figure 7. (A) Representative PET images of WT and MAGL-KO mouse brains at 30–120 min after intravenous injection of ^{18}F-M$_3$. (B) TACs for multiple brain regions after administration of ^{18}F-M$_3$ (n = 4 in each group). FCX, frontal cortex; STR, striatum.

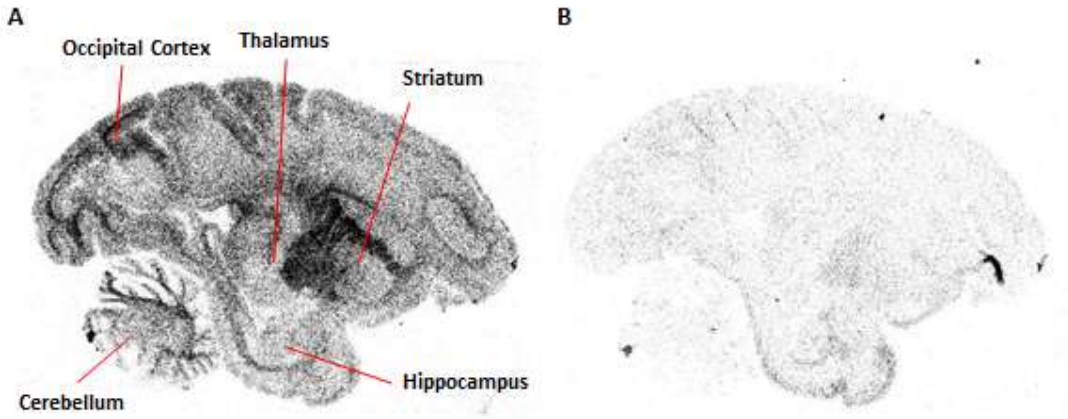

Supplemental Figure 8. *In vitro* autoradiogram of rhesus monkey brain sections. Incubation of ^{18}F-T-401 (0.5 nM) (A) and co-incubation of ^{18}F-T-401 (0.5 nM) and JW642 (10 μM) (B).

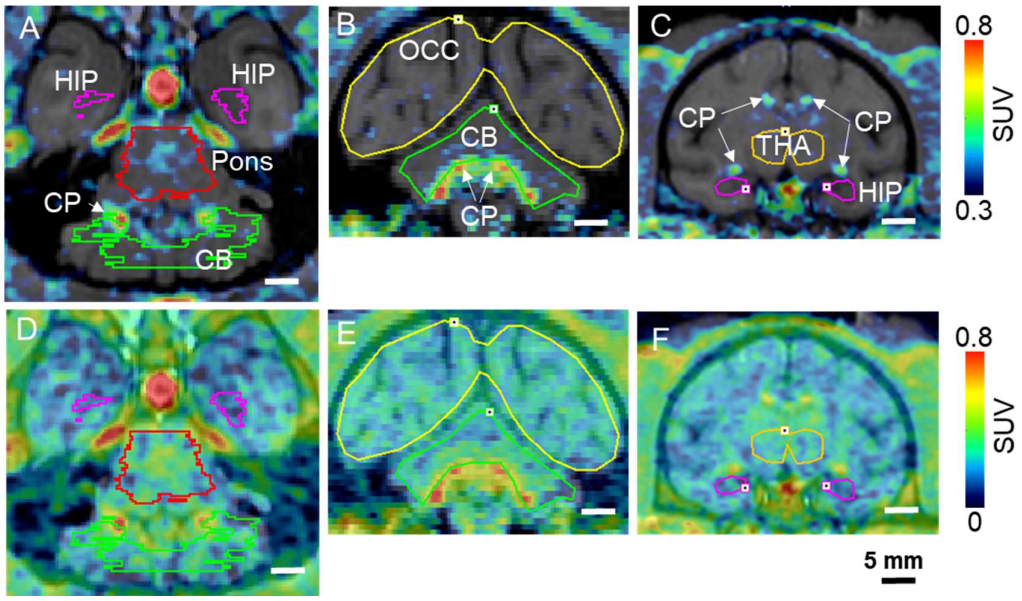

Supplemental Figure 9. Definition of ROIs on PET/MRI maps. Top row images (A - C) with a higher SUV cut-off were generated to visualize the radioactivity accumulation in choroid plexus (CP) and its spillover in neighboring tissues, and bottom row images (D - F) with a lower cut-off were displayed to evaluate the radioactivity retention in the brain parenchyma. The radioactivity spilled from CP in the fourth ventricle into the ventral part of the cerebellum (CB; A, B). By contrast, the spillover of the CP radioactivity into the pons (A) and hippocampus (HIP; C) are much less profound. Moreover, the ROI in the thalamus (THA) was initially drawn on the dorsal part to avoid significant radioactivity spill-in from CP (C). The radioactivity retention in the dorsal part of CB, which is distant from CP, was minimally affected by the spillover from CP. Accordingly, the retention was almost equivalent to that of the occipital cortex (OCC), where the spill-in was negligible.

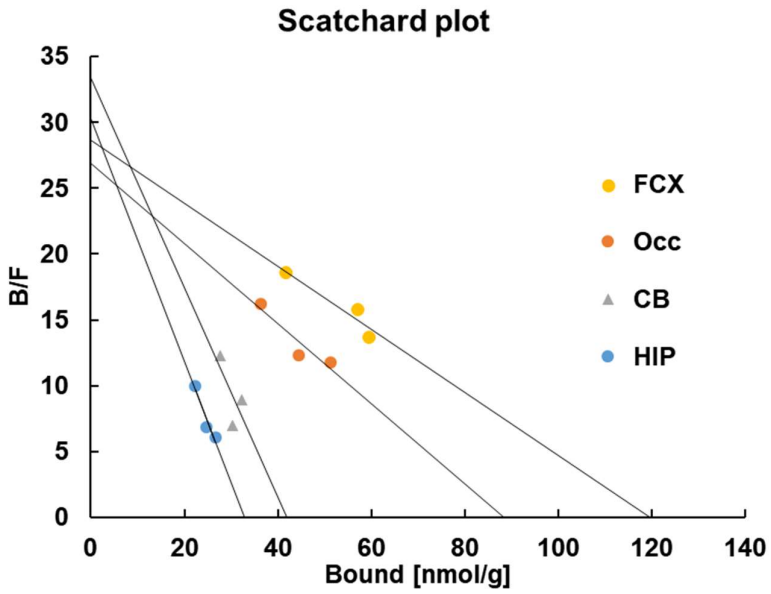

Supplemental Figure 10. Scatchard plot to determine K_D and B_{max} values from baseline [^{18}F]T-401-PET data. FCX, frontal cortex; OCC, occipital cortex; CB, cerebellum; HIP, hippocampus. Solid lines in the plot indicate regressions.